The S_0 State EPR Signal from the Mn Cluster in Photosystem II Arises from an Isolated $S = {}^1/_2$ Ground State†

Karin A. Åhrling,‡ Sindra Peterson, and Stenbjörn Styring*

Department of Biochemistry, Center for Chemistry and Chemical Engineering, Lund University, PO BOX 124, S-221 00 Lund, Sweden

Received January 15, 1998; Revised Manuscript Received March 24, 1998

ABSTRACT: During oxygen evolution, the Mn cluster in Photosystem II cycles through five oxidation states, S_0-S_4. S_0 and S_2 are paramagnetic, and can be monitored by electron paramagnetic resonance (EPR). Recently a new EPR signal from the S_0 state was discovered [Åhrling et al. (1997) *Biochemistry 36*, 13148−13152, Messinger et al. (1997) *J. Am. Chem. Soc. 119*, 11349−11350]. Here, we present a well-resolved S_0 spectrum, taken at high power and low temperature. The spectrum is wider and more resolved than previously thought, with structure over more than 2500 G, and appears to have at least 20 reproducible peaks on each side of $g = 2$. We also present the temperature dependence of the unsaturated S_0 signal amplitude. A linear relationship was found between signal intensity and reciprocal temperature ($1/T$) in the region 5−25 K, clearly extrapolating to 0. This obeys the Curie law, indicating that the S_0 state is a ground $S = {}^1/_2$ state with no thermally accessible excited state. The data are consistent with a minimum energy gap of 30 cm^{-1} between the ground and first excited states.

Photosystem II (PSII)[1] in plants, algae, and prokaryotic organisms catalyzes the light-dependent electron transfer from water to plastoquinone. In this process water is oxidized to molecular oxygen. The excited primary electron donor, P680, ejects an electron which reduces Q_A, the first quinone acceptor. $P680^+$ is then quickly rereduced by a redox-active tyrosine (Y_Z) situated close, thereby ensuring stable charge separation. $Y_Z{}^{ox}$ is in turn reduced by a nearby cluster of four Mn ions, often called the oxygen-evolving complex (OEC) because it catalyzes the oxidation of water. The OEC is capable of storing, in a cyclic manner, four oxidizing equivalents before it oxidizes water to molecular oxygen and the cycle starts over. The intermediate oxidation states of the OEC are denoted S_0-S_4, where the subscript refers to the number of electron holes stored (*1*). For recent reviews see refs 2−5.

Until photosystem II, with an intact OEC, has been structurally determined, study of this enzyme relies on spectroscopy. Here EPR spectroscopy is an excellent probe for the structure and function of the paramagnetic redox states in the S cycle. The S_2 state is paramagnetic and gives rise to a complex Mn hyperfine structured EPR spectrum (the multiline signal) (*6*) arising from, at least, an antiferromagnetically coupled redox-active $Mn^{III}-Mn^{IV}$ dimer, as well as a broad unstructured EPR spectrum centered around $g = 4$ (the 4.1 signal), with a peak-to-peak width at X-band of 350 G (*7*, *8*).

For a long time, this was the only S state from which EPR signals from a fully functional OEC were visible. Recently the S_1 state also became accessible to EPR studies, when Yamauchi et al. (*9*) were able to confirm the results reported by Dexheimer and Klein (*10*) of an EPR signal from the S_1 state observed by parallel polarization EPR studies. The properties of this signal are consistent with the S_1 state arising from a weakly antiferromagnetically coupled redox-active $Mn^{III}-Mn^{III}$ dimer (*5*). It is a broad, featureless signal with a peak-to-peak width of 600 G.

The S_0 state is two steps before the S_2 state in the oxidation cycle and is therefore two electrons more reduced. As a consequence it is predicted to be paramagnetic, corroborated by (*11*) the microwave power saturation behavior of signal II_{slow}. This EPR signal arises from a redox-active tyrosine in PSII, $Y_D{}^{ox}$, the relaxation of which was enhanced in the S_2 and S_0 states, compared with the S_1 state (*11*). The S_0 state is indeed paramagnetic, and recently, an EPR spectrum was discovered independently by two groups (*12*, *13*). We have demonstrated that the new EPR signal arises from a fully active, oscillating OEC, as the signal returns on the second turnover of the enzyme (*12*). Essential for its observation is the addition of a small amount (1−3%, v/v) of methanol to the EPR samples (*12*−*14*).

The S_0 signal is in many ways similar to the S_2 state multiline signal. It is a wide hyperfine structured Mn signal arising from an antiferromagnetically coupled system with net spin $S = {}^1/_2$. However, the overall width and peak separation is consistent with the S_0 state signal arising from the redox-active dimer of the OEC in a $Mn^{II}-Mn^{III}$ oxidation state (*12*−*14*). Furthermore, its decay at room temperature is 10 times slower than that in the S_2 state (*12*). Recent results also indicate that the S_0 state signal relaxes differently than the S_2 multiline signal (Peterson, Åhrling, and Styring, manuscript in preparation).

† The work was supported by the Swedish Natural Science Research Council, the Knut and Alice Wallenberg Foundation, and the Crafoord Foundation.

‡ Current address: Department of Chemistry, Faculty of Science, Australian National University, Canberra 0200, Australia.

[1] Abbreviations: Chl, chlorophyll; DMSO, dimethyl sulfoxide; EPR, electron paramagnetic resonance; OEC, oxygen-evolving complex; PPBQ, phenyl-*p*-benzoquinone; PSII, Photosystem II; Y_D, tyrosine D; Y_Z, tyrosine Z.

S0006-2960(98)00117-2 CCC: $15.00
Published on Web 05/14/1998

The S_0 state EPR signal provides a new probe to the function of the Mn cluster. It is therefore important to elucidate its physical and biochemical properties in great detail to cast further light on the chemistry occurring in the oxygen-evolving cycle. Here we report the temperature dependence of the S_0 state EPR signal and compare it to the temperature dependence of the S_2 state multiline signal.

MATERIALS AND METHODS

PSII-enriched membrane fragments were prepared from spinach as in Pace et al (*15*). Oxygen evolution was measured using a Clark oxygen electrode with phenyl-*p*-benzoquinone (PPBQ) as electron acceptor. The membranes' oxygen-evolving capacity was 400 μM O_2/mg of Chl/h.

EPR samples were made up to 3.5 mg of Chl/mL in a buffer containing 400 mM sucrose, 15 mM NaCl, 10 mM $MgCl_2$, 20 mM MES, pH 6.0, with 3% (v/v) methanol. The samples were incubated in the dark at room temperature for 10 min and given a saturating flash from a Nd:YAG laser (6 ns, 450 mJ, at 532 nm). After this preflash, given in the absence of electron acceptors to allow efficient recombination, the samples were left to equilibrate at room temperature in the dark for 15 min. The samples, now synchronized in the S_1 state (*12*, *16*) were given 0, 1, or 3 flashes one minute after PPBQ (0.5 mM in dimethyl sulfoxide) had been added. After the actinic flashes, the samples were frozen within 1−2 s in an ethanol/solid $C0_2$ slurry and then rapidly transferred to liquid nitrogen.

Continuous wave EPR spectra were recorded at liquid helium temperatures with a Bruker 380E spectrometer fitted with an Oxford Instruments cryostat and temperature controller, model ITC 503. Spectrometer conditions are given in the figure captions. EPR spectra were treated using WinEPR software from Bruker.

Data Analysis. The intensity of the EPR signals at different microwave powers was measured on a set of three peaks for both the S_0 (Figure 1) and S_2 state EPR signals. These peaks were chosen where the two signals have little overlap (Figures 2 and 3, insets). This is particularly important for the S_0 state signal as it will always contain some contribution of the S_2 state (at least 8% (*12*)). At low temperature, (T < 7K), the analysis can be extended also to partly overlapping lines, but at higher temperatures, (T > 9K), the S_2 state signal, although it only amounts to a few percent of the centers, makes reliable analysis of overlapping lines impossible. The region for the S_2 state peaks has a small underlying contribution from Cytochrome b_{559} at g = 2.2 (*17*). This did not affect the results, which was confirmed when we recalculated the signal intensity at various powers and temperatures, using different peaks, and found the correlation good.

Temperature Calibration. To evaluate the temperature dependence data it was necessary to check the accuracy and calibration in the temperature regulation and in the measurement system and the method of analysis. In this study we used two standards to calibrate our temperature system, the rhombic Fe^{3+} EPR signal present in PSII samples (*15*, *17*) and the $g \approx 6$ Fe^{3+} signal from myoglobin (*18*, *19*). The inorganic Fe^{3+} present in PSII material gives a sharp EPR signal centered at g = 4.28 which has been shown to arise from the middle Kramers doublet ($\pm^1/_2$) with zero field-splitting parameters $E/D = {}^1/_3$, $D \neq 0$, where the doublets

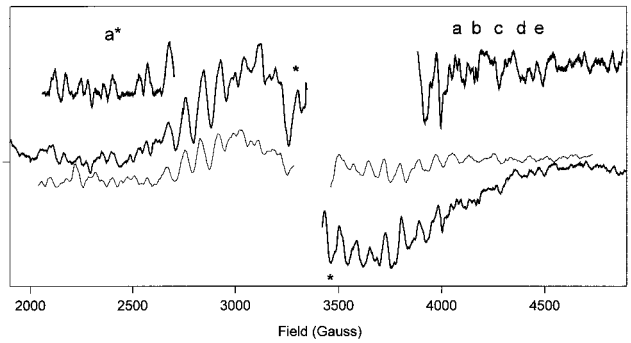

FIGURE 1: High-resolution S_0 state EPR spectrum over 3000 G (bold). The spectrum was recorded using 10 G modulation amplitude. For clarity we show our earlier published spectrum (*12*) (fine line), which shows that the many peaks we can resolve in the high-resolution spectrum are real. (The previously published spectrum has been cut at g = 2 and pushed together to fit within the high-resolution spectrum. Its overall shape with the underlying broad component (discussed in ref 12) is therefore not predominant, but individual peaks are.) Most of these were visible in our earlier spectrum but could not be unambiguously assigned at that time. The amplified (×2) spectra show parts of the main spectrum where we have subtracted a splined baseline to improve the visualization of the spectral peaks. The letters identify the peaks previously assigned. The peaks marked with (*) were not visible earlier due to overmodulation. The spectra shown are illuminated-dark difference spectra. The high-resolution S_0 spectrum has also had a 10% contribution of S_2 state spectrum (recorded under the same conditions) subtracted from it. In the central part of the spectrum the large EPR signal from Y_D^{ox} (signal II_{slow}) has been omitted. The spectrometer conditions were the following: frequency, 9.44 GHz; modulation frequency, 100 MHz; modulation amplitude, 10 G; microwave power, 57 mW; temperature, 7 K. The fine line spectrum is the 8 flash S_0 spectrum as presented in ref 12, acquired with modulation amplitude 20 G and aligned with the current spectrum at g = 2. In the 8 flash spectrum the region 3000−3300 G is less resolved due to subtraction artifacts.

are separated by 2.6 K (*20*). We measured this signal in our PSII samples between 5 and 30 K (Figure 5, inset). Using the expression $I_0 = C/T[e^{-\theta/T}/(1 + e^{-\theta/T} + e^{-2\theta/T})]$, the temperature dependence of the rhombic iron signal could be fitted assuming θ = 2.6 K and C (initial intensity, specific to sample and cavity) in arbitrary units. Our data are shown in the inset in Figure 5 and we estimate the accuracy of the temperature measurement to be ±0.3 K. We were not able to measure the signal at nonsaturating powers below 5 K. We also used the $g \approx 6$ signal from Fe^{3+} in myoglobin (*20*) as an external standard to quantify the error in temperature measurement. Myoglobin was added in a capillary inside the quartz EPR tube and its temperature dependence measured at the same time as that of the S_2 state. (This method was suggested to us by Dr. Örjan Hansson, Göteborg.) The temperature dependence fit well with the zero field-splitting parameter established by Scholes et al. (*18*) (D = 9.14 cm^{-1}), and we, also in this case, estimate the accuracy of the temperature measurement to be ±0.3 K in the temperature range 4.5−25 K (not shown).

RESULTS AND DISCUSSION

A Highly Resolved S_0 State EPR Spectrum. Figure 1 shows a detailed illuminated-minus-dark S_0 signal accumulated at comparatively high microwave power (57 mW) at the observation temperature 7 K. The high power was chosen as relaxation studies have determined that the signal does not saturate under the conditions of our instrument

(microwave power at half saturation at 7 K is 250 mW, (Peterson, Åhrling, and Styring, manuscript in preparation)). The S_2 signal, on the other hand, saturates, and any contribution from it is therefore diminished under these conditions. The low modulation amplitude used in this spectrum (10 G) permits the observation of an additional peak on either side of signal II_{slow}, which had previously disappeared into the overmodulated radical signal (*, Figure 1). The spectrum also confirms the structure previously seen at the edges of the spectrum (*12*), although with this modulation the peaks are better resolved. In particular, the peaks surrounding feature *a** in Figure 1 seem reproducible from sample to sample although they were not assigned in our earlier published spectrum (Figure 1, gray; which was recorded at a higher modulation amplitude). In addition there are several more peaks that appear beyond those previously identified. We observe structure, well identified above the noise level of the spectrum, over a width of almost 3000 G. By comparing the plots of signal intensity versus microwave power at various temperatures for the S_0 and S_2 state spectra (Figures 2 and 3) one can observe that at conditions of high power (>100 mW) and low temperature (5 K) any contribution from the S_2 state signal that may be present virtually disappears from the third flash S_0 state spectrum. Under these conditions, where we also expect that other paramagnetic centers which may contribute structural features are saturated, the structures at the edges remain. This is not a clear identification of the spectral edges, but an indication that the S_0 state EPR spectrum is even wider than previously suggested. Messinger et al. (*13*) identified 16 peaks on the high field side of the S_0 spectrum and nine at the low field end. This difference is less likely to be real as the *g* value needed to explain such an anisotropy will need to be ~1.86, at least in one (*x* or *y*) direction of the *g* tensor. In the spectrum presented in Figure 1 we identify about 20 peaks on either side of the $g = 2$ region of the spectrum. The peaks were observed by us earlier (*12*) although only some were assigned with certainty at that time. The peaks previously assigned are marked in Figure 1, which also shows our earlier published spectrum in which the peaks were first assigned, for comparison with the high-resolution spectrum. We are not certain that this is the total picture. A clear identification of features in the spectral edges will only be possible when spectra from several microwave frequencies can be compared. This is currently in progress.

Temperature Dependence Studies. Here we have studied the behavior of the unsaturated S_0 state signal intensity with variation in temperature and compared it with the S_2 state multiline signal. For each temperature the S_0 or S_2 state EPR signals (3 flash and 1 flash samples, respectively) were measured at several microwave powers. Figure 2 shows the plot of signal intensity versus the square root of the applied microwave power for the S_0 state signal at 4.2, 7, 12, and 20 K. This signal does not readily saturate at these temperatures. It has a half saturation power of about 250 mW at 7 K. The initial slopes of the plots are therefore relatively easy to determine.

Figure 3 shows the saturation plots for 4.2, 7, 12, and 20 K for the S_2 state signal. In contrast to the behavior of the S_0 state signal, the S_2 state multiline signal saturates more easily at temperatures below 5 K ($P_{1/2}$ at 7 K is 85 mW in the presence of methanol).

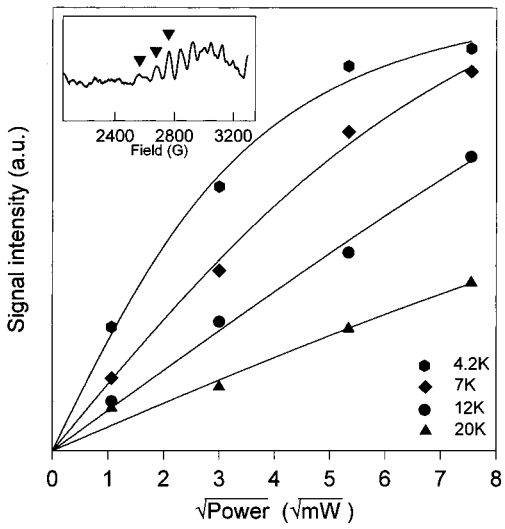

FIGURE 2: Microwave power dependence of the S_0 state EPR signal: signal intensity (measured as the summed amplitudes of the three peaks indicated in the inset) versus the square root of the applied microwave power (√mW). The spectra were recorded at different temperatures (4.2, 7, 12, 20 K) in the same sample using 20 G modulation amplitude.

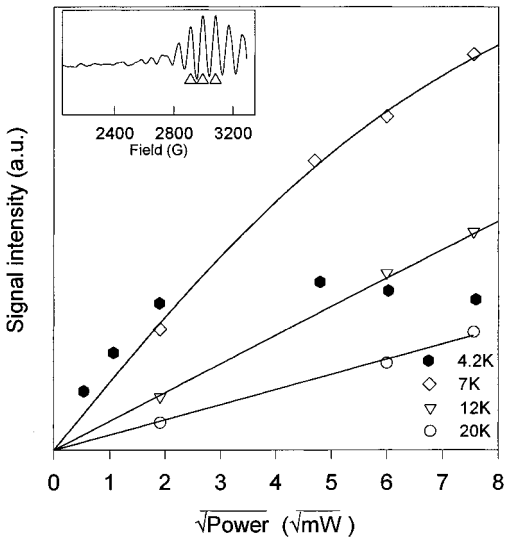

FIGURE 3: Microwave power dependence of the S_2 state EPR signal: signal intensity (measured as the summed amplitudes of the three peaks indicated in the inset) versus the square root of the applied microwave power (√mW). The spectra were recorded at different temperatures (4.2, 7, 12, 20 K) in the same sample using 20 G modulation amplitude.

The true unsaturated signal intensity (I_0) is obtained by fitting the power saturation data at each temperature to

$$I = \frac{I_0\sqrt{P}}{\sqrt{(1 + P/P_{1/2})^b}} \quad (1)$$

where *I* is the signal intensity observed at a particular power, *P* is the microwave power, $P_{1/2}$ is the half-saturation power, and *b* is the "inhomogeneity parameter" (*21*) which for an inhomogeneously broadened line is 1. In the low power limit $I = I_0\sqrt{P}$, and I_0 is then the initial slope as the applied microwave power approaches 0. Each temperature curve was fitted with eq 1 and we thus obtained the slope, extrapolated to the unsaturated region.

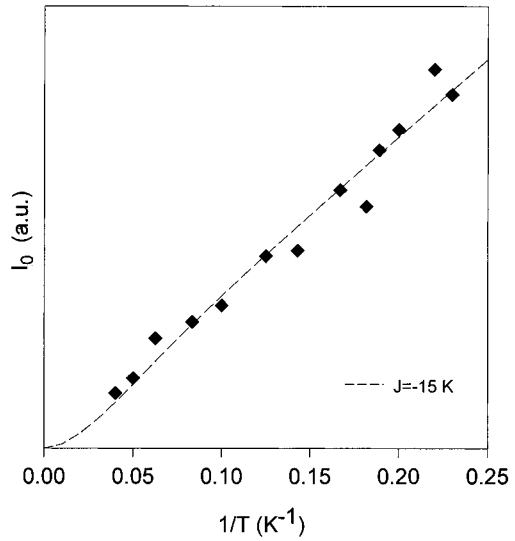

FIGURE 4: Curie plot showing the temperature dependence of the S_0 state EPR signal. The nonsaturated signal amplitude at each temperature is obtained from the data in Figure 2 (and a full temperature series, acquired simultaneously) using eq 1, see text. The line represents the lower limit of $|J|$ fitted to the measured points using eq 2 with $J = -15$ K.

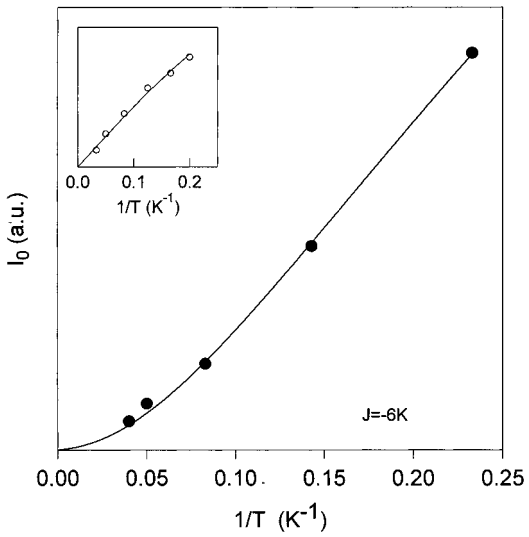

FIGURE 5: Curie plot showing the temperature dependence of the S_2 state multiline signal. The nonsaturated signal amplitude at each temperature is obtained from the data in Figure 3 (and a full temperature series, acquired simultaneously) using eq 1, see text. The line represents the best fit of the measured points using eq 2 with $J = -6$ K. The inset shows the data for the $g = 4.3$ rhombic Fe^{3+} iron EPR signal present in PSII membrane fragments. The curve is a fit with $\theta = 2.6$ K. This signal was used as an internal temperature standard (see Materials and Methods).

The Curie plot, I_0 vs $1/T$, for the S_0 state signal is shown in Figure 4. The temperature dependence appears to follow Curie dependence in that it is linear over the measured temperature range, 4−25 K, and clearly extrapolates to 0. This behavior is different from the temperature dependence of the S_2 multiline signal, which does not extrapolate linearly to 0 (Figure 5, see below). The clear Curie temperature dependence of the S_0 signal indicates that the S_0 state is an isolated $S = {}^1/_2$ ground state. In other words, there appears to be no thermally accessible excited state $S = {}^3/_2$ signal under these conditions.

The Mn cluster, at least in the S_2 state, is often thought to contain two dimers, coupled weakly to each other. One of these is considered to be redox-active (*5*, *22*), while the other probably does not alter its valence during the cycling of the OEC. Our recent analysis of the S_0 state spectrum (*12*) suggests that the S_0 state also fits this model. To get an estimate of the strength of the coupling between the Mn in the redox-active dimer, as well as a lower limit to the Curie behavior, we assume for simplicity that the behavior is dominated by an antiferromagnetically coupled redox-active dimer, with a net $S = {}^1/_2$ state, in both S_0 and S_2 (as the redox-inactive dimer may be assumed to have net spin $S = 0$). This model is equivalent to the model with two exchange coupled spins described elsewhere (*9*, *15*). We obtain a fit to the following equation:

$$I_0 = \frac{C}{T}\frac{(2S+1)\exp(-E_S/kT)}{\sum_j (2j+1)\exp(-E_j/kT)} \qquad (2)$$

where the exchange Hamiltonian has the form $H = -2JS_1 \cdot S_2$, ($S_1 = {}^5/_2$, $S_2 = 2$ for the S_0 state; $S_1 = 2$, $S_2 = {}^3/_2$ for the S_2 state, and S_1 and S_2 are the spins of the individual Mn ions), giving the energy levels: $E_j/J = S_1(S_1+1) + S_2(S_2+1) - S_T(S_T+1)$ and $S_T = {}^1/_2 - {}^9/_2$ for S_0 and $S_T = {}^1/_2 - {}^7/_2$ for S_2; C is an arbitrary constant.

The temperature dependence of the S_0 state signal (Figure 4) shows that the S_0 signal comes from a ground ($S = {}^1/_2$) state. The data could be fitted with eq 2 assuming a value of $|J| > 15$ K. Figure 2 shows the fits for $J = -15$ K, which represents a lower limit of $|J|$. This implies that the energy gap ($3J$) to the first excited state would lie at least 30 cm^{-1} above the ground state and would not be thermally accessible.

Figure 5 shows the Curie plot for the S_2 state multiline in the presence of methanol. The S_2 multiline, in contrast to the S_0 state signal, is not strictly Curie-dependent. We observe Curie dependence below 20 K, but deviation above 20 K as the curve does not extrapolate to 0. The data can be fitted with $J = -6$ K. Pace et al. (*15*) have studied the temperature dependence of the S_2 state EPR signal and find a higher value for J ($J \approx -13$ K) also with no deviation from Curie behavior in the temperature range measured (5−18 K) in the presence of methanol. In the absence of methanol, however, they found $J \approx -3$ K. Our data falls somewhere between the two results of Pace et al. (*15*). Other groups have studied the temperature dependence in the presence of ethylene glycol or ethanol (*19*, *23*, *24*) and find a temperature dependence similar to that reported here. Whereas all groups report Curie dependence over some temperature range (typically 5−15 K), there are variations in the results and strict Curie law behavior is not often observed. We conclude that these studies are strongly dependent on sample preparation protocols and additions (e.g., ethylene glycol, ethanol, or methanol) made to the buffers. They are, however, reproducible for a given protocol.

Thus, our temperature study clearly reveals significant differences between the S_0 state signal and S_2 multiline signal. In S_0 the temperature dependence follows strictly Curie dependence, while most measurements in the S_2 state reveal clear deviations from Curie dependence in the higher temperature limit (above 15 K).

Table 1: Exchange Couplings in the Different Observable S States in the OEC; Effect of Methanol

S state	J (cm^{-1}) with methanol	J (cm^{-1}) without methanol
S_0 (this work)	$\sim -12^a$	*b*
S_1 (*9*)	$\sim -5^c$	−0.87
S_2 multiline (*15*)	−10	−2
S_2 multiline (this work)	~ -4	nd[d]

[a] Estimated from the lower limit of the fit of the exchange coupling to the data. [b] In the absence of methanol the S_0 state EPR signal has not been observed. [c] Estimated as the lower limit of J at which which the S_1 state would not be observed. [d] nd = not determined.

Effect of Methanol. The observation of the S_0 state signal is dependent on the addition of a few percent of methanol. At present we have not been able to observe the signal with the addition of other small monoalcohols. Thus it is tempting to infer that methanol can gain access to the OEC and interact directly, perhaps by replacing water, while other alcohols cannot. In this respect it is useful to note that methanol has been shown to replace water in a synthetic Mn dimer (*25*). Interactions of this nature have also been observed in another system. Hägerhäll et al. (*26*), while studying a tri-iron−sulfur cluster in *Bacillus subtilis*, observed that methanol (0.2−1% v/v) greatly reduced the line width of the iron−sulfur EPR spectrum. The effect was specific to methanol and they concluded that methanol was able to interact directly with the iron−sulfur cluster. They also observed that methanol increased the relaxation time of the signal, contrary to what is observed in the S_2 state (*15*), (Peterson, Åhrling, and Styring, manuscript in preparation). In the S_2 state of the OEC, the addition of small monoalcohols to the buffer is known to shift the equilibrium between the simultaneous observation of $g = 4$ and multiline signals, such that only the multiline signal is observed. Pace et al. (*15*) calculate the exchange coupling to be ~ -2 cm^{-1} without alcohol and ~ -10 cm^{-1} with alcohol (i.e., the gap to the next excited state is ∼6 and ∼30 cm^{-1}, respectively). A similar gap is inferred for the S_0 state (in the presence of methanol) from the size of the exchange coupling given by the fit to the Curie plot (see above, Figure 4). A much smaller (antiferromagnetic) exchange coupling is reported for the S_1 state signal, $J = -0.87$ cm^{-1} (*9*). This is an excited-state signal and is not observed in the presence of methanol, and Yamauchi et al. estimate that the exchange coupling in the presence of methanol is at least -5 cm^{-1}. Table 1 summarizes the exchange couplings found in samples with or without the addition of methanol in the S_0, S_1, and S_2 states. The effect of alcohol appears to be the same in the S_2 and S_1 states. If extendable also to the S_0 state, this would predict a small antiferromagnetic coupling or perhaps even a ferromagnetic coupling for the S_0 state without alcohol. Furthermore, in the S_2 state it is worth noting that the latter effect appears to be independent of the type of alcohol as it has been observed with both ethanol and propanol (4% v/v) (*27*), where direct interaction of the alcohol is less likely. Biochemical studies of the S_0 state in the presence of various alcohols are in progress.

CONCLUSION

We have found that the S_0 state EPR signal arises from an $S = {}^1/_2$ ground state. The temperature dependence of the signal obeys the Curie law which implies that there is no thermally accessible excited-state signal. This is turn implies a relatively strong intradimer coupling in the redox-active dimer, estimated to be ~ -12 cm^{-1}. The highly resolved S_0 state EPR spectrum shows ∼20 peaks in the low field and high field portions of the spectrum indicating structural complexity and additional width of the spectrum.

ACKNOWLEDGMENT

We acknowledge valuable discussions with Y. Frapart, Ö. Hansson, and R. J. Pace.

REFERENCES

1. Kok, B., Forbush, B., and McGloin, M. (1970) *Photochem. Photobiol. 11*, 457−475.
2. Debus, R. J. (1992) *Biochim. Biophys. Acta 1102*, 269−352.
3. Britt, R. D. (1996) in *Advances in Photosynthesis; Oxygenic Photosynthesis: The Light Reactions* (Ort, R., and Yocum, C. F., Eds.) pp 137−164, Kluwer Academic Publishers, Dordrecht.
4. Diner, B. A., and Babcock, G. T. (1996) in *Advances in Photosynthesis; Oxygenic Photosynthesis: The Light Reactions* (Ort, R., and Yocum, C. F., Eds.) pp 214−247, Kluwer Academic Publishers, Dordrecht.
5. Yachandra, V. K., Sauer, K., and Klein, M. P. (1996) *Chem. Rev. 96*, 2927−2950.
6. Dismukes, G. C., and Siderer, Y. (1981) *Proc. Natl. Acad. Sci. U.S.A. 78*, 274−278.
7. Casey, J. L., and Sauer, K. (1984) *Biochim. Biophys. Acta 767*, 21−28.
8. Zimmerman, J., and Rutherford, A. W. (1984) *Biochim. Biophys. Acta 767*, 160−167.
9. Yamauchi, T., Mino, H., Matsukawa, T., Kawamori, A., and Ono, T. (1997) *Biochemistry 36*, 7520−7526.
10. Dexheimer, S. L., and Klein, M. P. (1992) *J. Am. Chem. Soc. 114*, 2821−2826.
11. Styring, S., and Rutherford, A. W. (1988) *Biochemistry 27*, 4915−4923.
12. Åhrling, K. A., Peterson, S., and Styring, S. (1997) *Biochemistry 36*, 13148−13152.
13. Messinger, J., Robblee, J., Yu, W. O., Sauer, K., Yachandra, V. K., and Klein, M. P. (1997) *J. Am. Chem. Soc. 119*, 11349−11350.
14. Messinger, J., Nugent, J. H. A., and Evans, M. C. W. (1997) *Biochemistry 36*, 11055−11060.
15. Pace, R. J., Smith, P., Bramley, R., and Stehlik, D. (1991) *Biochim. Biophys. Acta 1058*, 161−170.
16. Styring, S., and Rutherford, A. W. (1987) *Biochemistry 26*, 2401−2405.
17. Miller, A.-F., and Brudvig, G. W. (1991) *Biochim. Biophys. Acta 1056*, 1−18.
18. Scholes, C. P., Isaacson, R. A., and Feher, G. (1971) *Biochim. Biophys. Acta 244*, 206−210.
19. Aasa, R., Andreasson, L.-E., Lagenfelt, G., and Vänngård, T. (1987) *FEBS Lett. 221*, 245−248.
20. Castner, T., Newell, G. S., Holton, W. C., and Slichter, C. P. (1960) *J. Chem. Phys. 32*, 668−673.
21. Rupp, H., Rao, K. K., Hall, D. O., and Cammack, R. (1978) *Biochim. Biophys. Acta 537*, 255−269.
22. Evelo, R. G., Styring, S., Rutherford, A. W., and Hoff, A. J. (1989) *Biochim. Biophys. Acta 973*, 428−442.
23. Vänngård, T., Hansson, Ö., and Haddy, A. (1992) in *Manganese Redox Enzymes* (Pecoraro, V. L., Ed.) pp 105−118, VCH, New York.

24. Britt, R. D., Lorigan, G. A., Sauer, K., Klein, M. P., and Zimmerman, J. (1992) *Biochim. Biophys. Acta 1040*, 95−101.
25. Randall, D. W., Gelasco, A., Caudle, M. T., Pecoraro, V. L., and Britt, R. D. (1997) *J. Am. Chem. Soc. 119*, 4481−4491.
26. Hägerhäll, C., Sled, V., Hederstedt, L., and Ohnishi, T. (1995) *Biochim. Biophys. Acta 1229*, 356−362.
27. Åhrling, K. A., and Pace, R. J. (1995) in *Photosynthesis: From light to biosphere* (Mathis, P. E., Ed.) Vol 2, pp 309−312, Kluwer Academic Publishers, Dordrecht.

BI980117O